

Circular RNA circ_SKA3 enhances gastric cancer development by targeting miR-520h

Chuntao Wang^{1*}, Hao Jiang^{2*}, Jiaqun Peng¹, Duanshun Weng¹, Yu Zhang¹, Yanxun Zhou³ and Qin Zhang¹

¹Department of Thyroid Gastroenterology and Thoracic Surgery, ²Department of Hepatopancreatobiliary Surgery and

³Department of Gastroenterology, Suizhou Central Hospital, Suizhou, Hubei, China

*Chuntao Wang and Hao Jiang contributed to this work equally as co-first authors

Summary. Purpose. To explore the mechanisms of action of circ_SKA3 in gastric cancer (GC), which are still not fully understood.

Methods. Subcellular localization assay was used to analyze the localization of circ_SKA3, and Actinomycin D assay was applied to confirm the stability of circ_SKA3. The levels of circ_SKA3, microRNA (miR)-520h, and cell division cycle 42 (CDC42) mRNA were gauged by quantitative real-time polymerase chain reaction (qRT-PCR). The protein levels of CDC42 and proliferating cell nuclear antigen (PCNA) were assessed by western blot. Cell proliferation, colony formation, cell cycle distribution, apoptosis, migration, and invasion were detected by 3-[4,5-dimethylthiazol-2-yl]-2, 5-diphenyltetrazolium bromide (MTT), 5-Ethynyl-2'-Deoxyuridine (EdU) incorporation, colony formation, flow cytometry, and transwell assays, respectively. Directed relationship between miR-520h and circ_SKA3 or CDC42 was verified by a dual-luciferase reporter assay. Mouse xenograft experiments were used to elucidate the impact of circ_SKA3 *in vivo*.

Results. Overexpression of circ_SKA3 was validated in GC tissues and cells. The down-regulation of circ_SKA3 suppressed proliferation, cell cycle progression, colony formation, migration, invasion, and promoted cell apoptosis *in vitro*, as well as weakening tumor growth *in vivo*. Circ_SKA3 directly bound to miR-520h, and circ_SKA3 regulated CDC42 expression through miR-520h. Circ_SKA3 exerted regulatory effects on GC cell behaviors by inhibiting miR-520h. Furthermore, CDC42 was a functional target of miR-520h in regulating GC cell behaviors.

Conclusion. Our findings established a strong molecular mechanism, the miR-520h/CDC42 axis, at least in part, for the oncogenic role of circ_SKA3 in GC.

Key words: Gastric cancer (GC), circ_SKA3, miR-520h, CDC42

Introduction

Gastric cancer (GC), a complicated heterogeneous disease, remains the fifth most prevalent malignancy, with more than 1 million new cases annually globally. Despite advances in diagnosis and treatment, GC ranked as the third leading cause of cancer death in 2018 (Bray et al., 2018; Smyth et al., 2020). Importantly molecular modulators of gastric tumorigenesis, including circular RNAs (circRNAs) and microRNAs (miRNAs), are under exploration (da Silva Oliveira et al., 2016; Li et al., 2020). Knowing the mechanisms of their actions would provide a novel opportunity to design molecularly targeted interventions against GC.

CircRNAs are natural RNA circles that are formed by the non-canonical back-splicing through exon or intron circularization (Kristensen et al., 2019). As one type of non-coding RNAs, circRNAs exert critical functions from normal development to disease partially by inactivating miRNAs (Dori and Bicciato, 2019). Recently, some circRNAs have been shown as oncogenic drivers or suppressors in various cancers, including GC (Fang et al., 2019; Li et al., 2020). Examples of tumor-driver circRNAs in GC include hsa_circ_0092303, which operates as a miR-331-3p sponge to up-regulate transforming growth factor beta receptor 1 (TGFB1), and hsa_circ_0008549, which controls Wnt family member 2 (WNT2) expression by directly pairing to miR-136-5p (Wang et al., 2019; Zhang et al., 2019). Conversely, the tumor-suppressor hsa_circ_0000993 is closely associated with overall survival of GC patients and impedes GC metastasis by sequestering miR-214-5p (Zhong et al., 2018). As for circRNA spindle and kinetochore associated complex subunit 3 (circ_SKA3, hsa_circ_0000467), produced by the back-splicing of SKA3, it has been predicted as a promising prognostic marker for GC patients (Chen et

Corresponding Author: Yanxun Zhou and Qin Zhang, Department of Thyroid Gastroenterology, Suizhou Central Hospital, No. 13, Second Street, Yunsanzhuyu, Country Garden, Chengnan New District, Zengdu District, Suizhou 441300, Hubei, China. e-mail: kpfq70u@163.com
DOI: 10.14670/HH-18-521



al., 2020) and established as an oncogenic factor in gastric tumorigenesis (Lu et al., 2019; Mo et al., 2020). Nonetheless, the molecular basis for the promoting effect of circ_SKA3 on GC is still not fully understood.

Frequent misregulation of miRNAs has been reported during gastric tumorigenesis (Alessandrini et al., 2018). For instance, miR-21 contributes to GC carcinogenesis through prostaglandin E2 (Qi et al., 2018). MiR-133a-3p can hamper GC cell growth and metastasis by inhibiting glutaminolysis mediated by autophagy (Zhang et al., 2018b). MiR-520h has been recently revealed to be implicated in human carcinogenesis (Wang et al., 2010; Su et al., 2017). Moreover, the down-regulation of miR-520h was discovered to be related to shorter time to progression in GC (Smid et al., 2016). However, relatively little is known about the precise action of miR-520h in gastric tumorigenesis.

Here, we set out to identify the molecular basis underlying the promoting effect of circ_SKA3 on GC. We showed that the regulatory axis of the miR-520h/cell division cycle 42 (CDC42), a potent oncogene in GC (Du et al., 2016; Zhu et al., 2019), represented an important downstream mechanism of circ_SKA3 function on GC progression.

Materials and methods

Patient specimens and cells

In this cohort study, 35 pairs of gastric primary tumors and nontumor gastric tissue samples (~1.5 cm away from tumors) from gastrectomy were collected from the same patients at Suizhou central hospital between May 2017 and August 2019. These patients had no history of other tumors or previous radiotherapy or chemotherapy before surgery. Fresh specimens were preserved in RNAlater (Qiagen, Manchester, UK) in a -80°C freezer (Thermo Fisher Scientific, Waltham, MA, USA) or embedded by paraffin after formalin fixing. Formalin-fixed paraffin-embedded specimens were used for Ki67 and GC-marked Villin staining by immunohistochemistry with antibodies specific for Ki67 (ab15580, 1:100 dilution; Abcam, Cambridge, UK) and Villin (MA5-12227, 1:100 dilution; Invitrogen, Paisley, UK) as described elsewhere. The Ethics Committee of Suizhou central hospital approved the use of these patient specimens, and all patients signed written informed consent. In this study, we obtained human AGS and HGC27 GC cells and gastric epithelial GES-1 cells from Procell (Wuhan, China) and propagated them as described (Tian and Yu, 2017; Wang et al., 2017). All cell culture reagents were provided by Gibco (Paisley, UK).

Subcellular localization assay

Separation and purification of cytoplasmic and nuclear RNA were done using the Cytoplasmic and

Nuclear RNA Purification Kit based on the manufacturer's instructions (Norgen Biotek, Thorold, ON, Canada). We used U6 and glyceraldehyde-3-phosphate dehydrogenase (GAPDH) as the nuclear and cytoplasmic controls, respectively.

Actinomycin D assay

The experiments were conducted by maintaining AGS and HGC27 cells in medium containing 2 mg/mL of Actinomycin D (GlpBio, Montclair, CA, USA) at 37°C for 0, 8, 16, and 24h.

Transient transfection of cells

CDC42 overexpressing plasmid was created by inserting the sequence of human CDC42 (Accession: NM_044472.3) synthesized by Ribobio (Guangzhou, China) into the pcDNA3.1 vector (Addgene, Cambridge, MA, USA) with EcoR I and Xba I sites. The negative control plasmid (pcDNA) was generated using the nontarget sequence as above. The following RNA species (Ribobio; sequences are provided in Table 1) were used: siRNA-circ_SKA3 (si-circ_SKA3), nontarget siRNA (si-NC), miR-520h mimic, negative control mimic (miR-NC mimic), miR-520h inhibitor (anti-miR-520h), and negative inhibitor control (anti-miR-NC). 200 ng of plasmid, 100 nM of siRNA, 50 nM of miRNA mimic or inhibitor was incubated with Lipofectamine 3000 (Invitrogen) and Opti-MEM (Invitrogen) before plating. AGS and HGC27 (1×10⁵ cells/well) plated in 6-well plates were incubated with the complex. We harvested the transfected cells for further studies after culturing for 48h.

Table 1. Primer sequences and oligonucleotide sequences for transfection.

	Sequence (5'-3')
circ_SKA3	Forward GGGACTTAAAAATGCGAGGA Reverse GCAACAGGAGGATCAGACAGA
SKA3 mRNA	Forward TGGACTTGAGCGGTACATCG Reverse TGGGGTTACAATTACGGGCT
CDC42	Forward TCCTGTTTGAAGCCTCTGCC Reverse AAGCCAGACCAAGTTCCTTT
miR-520h	Forward GCCGAGACAAAGTGCTTCCC Reverse CTCAACTGGTGTCTGGGA
GAPDH	Forward GACAGTCAGCCGCATCTTCT Reverse GCGCCCAATACGACCAAAATC
U6	Forward CTCGCTTCGGCAGCACA Reverse AACGCTTCACGAATTTGCGT
si-circ_SKA3	GCUUCUUGUCUGUGUACUUUU
si-NC	AAGACAUGUGUGUCCGCCTT
miR-520h mimic	ACAAAGUCUUCUUUAGAGU
miR-NC mimic	ACGUGACACGUUCGGAGAATT
anti-miR-520h	ACUCUAAAGGGAAGCACUUUGU
anti-miR-NC	CAGUACUUUUGUGUAGUACAA

Effect of circ_SKA3 on GC development

Quantitative real-time polymerase chain reaction (qRT-PCR)

Total RNA of cells and tissues was extracted using the GeneALLR RiboEx Kit (GeneAll Biotechnology, Seoul, South Korea) and quantified spectrophotometrically using the Picodrop-100 (PicoDorp, Hinxton, UK). To assess the expression of circ_SKA3, SKA3, and CDC42 mRNAs, cDNA synthesis was performed by PrimeScript RT Kit (TaKaRa, Beijing, China) using 2 µg of total RNA and random hexamers. To quantify miR-520h, 1 µg of total RNA and miRNA-specific stem loop RT primers (Qiagen) were used to synthesize cDNA using the miScript RT Kit (Qiagen). qRT-PCR was performed in triplicate using SYBR Premix ExTaq Kit (TaKaRa) on a light cycler 96 (Roche, Penzberg, Germany). GAPDH or U6 was used as a housekeeping control to correct for differences in the amount of RNA in each sample. Primers are provided in Table 1. Relative fold changes were calculated by the $2^{-\Delta\Delta C_t}$ method (Jaca et al., 2017).

5-Ethynyl-2'-Deoxyuridine (EdU) assay

The assay was performed to evaluate cell proliferation using the EdU DNA Cell Proliferation Kit as described by the manufacturers (Ribobio). Briefly, transfected cells were plated in 96-well plates at 1×10^4 cells per well and then incubated with 50 µM of EdU for 2 h. After being fixed with 4% paraformaldehyde (Ribobio), the cells were stained with 1× Apollo solution for 30 min. After that, 1× Hoechst 33342 was added to visualize the nuclei. Stained cells were analyzed under a fluorescent microscope (Olympus, Tokyo, Japan) and the percentage of EdU-positive nucleus (red) relative to blue fluorescent nucleus was determined.

Cell proliferation and colony formation assays

For proliferation assays, we plated transfected cells at 1×10^3 cells per well in 96-well dishes, performed the 3-[4,5-dimethylthiazol-2-yl]-2, 5-diphenyltetrazolium bromide (MTT, Abcam) assay at the indicated time point, and measured the absorbance at 570 nm using the Infinite M200 Pro plate reader (Tecan, Shanghai, China). For colony formation assays, we plated transfected cells at a density of ~120 cells/well in 6-well dishes, stained the cells with 0.1% crystal violet (Genomeditech, Shanghai, China) 14 days later, and counted the number of colonies (>50 cells) using the Image J software (National Institutes of Health, Bethesda, MD, USA) in 10 random fields.

Flow cytometry for cell cycle distribution and apoptosis

For cycle distribution assays, we harvested transfected cells (2×10^5) by low-speed centrifugation and stained the cells with 5 µL of propidium iodide (PI, 50 µg/mL, Invitrogen). For apoptosis assays, we collected 2×10^5 cells after various transfections and

stained them using 10 µL of fluorescein isothiocyanate (FITC)-labeled Annexin V (Thermo Fisher Scientific) and 5 µL of PI. After 15 min incubation in the dark, the data were acquired by the MACSQuant flow cytometer (Miltenyi Biotec GmbH, Bergisch Gladbach, Germany) and expressed as the percentage of total cells.

Transwell migration and invasion assays

For migration studies, we seeded transfected cells onto the inserts with 8 µm pores in 24-transwell plates (Millipore, Shanghai, China) at 5×10^4 cells/well. For invasion studies, we plated cells after transfection onto the Matrigel-precoated insert membranes (Millipore) at 1×10^6 cells/well. In the lower chambers, we added 700 µL of complete medium. After being stained with 0.1% crystal violet, the cells on the lower surface were photographed and 10 random fields of each sample were counted microscopically at 100× magnification.

Western blot

Total protein of cells and tissues was prepared using the RIPA buffer (Invitrogen) plus protease inhibitors (Roche). SDS-polyacrylamide gel electrophoresis was conducted using the protein (50 µg each sample), and the resulting gel was electroblotted onto Clear Blot membrane-p (ATTO, Toyko, Japan). The following antibodies (Abcam) were used: proliferating cell nuclear antigen (PCNA, ab29, 1:200 dilution), CDC42 (ab41429, 1:500 dilution), GAPDH (ab8245, 1:5,000 dilution), and IgG secondary antibody labeled by horseradish peroxidase (ab6728, 1:5,000 dilution). Signals were developed using the Clarity Western ECL Substrate (Bio-Rad, Glattbrugg, Switzerland) and band intensity was evaluated with the Image J software.

Bioinformatics and dual-luciferase reporter assay

The targeted miRNAs of circ_SKA3 and miR-520h targets were searched using the starBase software at <http://starbase.sysu.edu.cn/>. The wild-type or mutant-type sequence of circ_SKA3 and CDC42 3'UTR in miR-520h complementary sites were inserted in the psiCHECK-2 vector (Promega, Beijing, China). AGS and HGC27 cells (1×10^5) were transfected with the reporter construct (200 ng), miR-520h mimic or control mimic (30 nM), and Lipofectamine 3000 in Opti-MEM (Invitrogen). Cells were harvested after 48h and assayed for luciferase activity on the Glomax 96 microplate Luminometer (Promega).

Lentiviral mediated knockdown of circ_SKA3

Lentiviral vectors encoding shRNA-circ_SKA3 (sh-circ_SKA3) and the control shRNA (sh-NC) were obtained from Genesee (Guangzhou, China). Lentiviruses were generated in 293T packaging cells by cotransfecting the vectors, psPAX2 (Addgene) and

Effect of circ_SKA3 on GC development

pMD2.G (Addgene). AGS cells were infected with the lentiviral supernatant for 48h in the presence of 8 $\mu\text{g}/\text{mL}$ polybrene (Genomeditech). Subsequently, puromycin (Genomeditech) was added into the media at a final concentration of 2 $\mu\text{g}/\text{mL}$, and transduced cells were selected over 96h.

Mouse xenograft assay

Mouse experiments and handling followed the approved protocol by the Animal Care and Use Committee of Suizhou central hospital. The subcutaneous xenograft tumors were generated by subcutaneous injections of AGS cells (5×10^6) stably transducing with sh-circ_SKA3 or sh-NC into the female BALB/c nude mice (6-week-old, Vital River Laboratory, Beijing, China; $n=6$ per group). Tumor growth was analyzed by periodically calculating tumor volume by the use of the formula $\text{length} \times \text{width}^2/2$. At the end point,

the subcutaneous tumors were harvested from the sacrificial mice for weight and further analysis. The tumors were used to measure circ_SKA3, miR-520h, and CDC42 expression by qRT-PCR and western blot as above. The tumors were also subjected to immunohistochemistry for the evaluation of Ki67, PCNA, matrix metalloproteinase 9 (MMP9) and CDC42 levels as previously reported (Korpál et al., 2011). The tissue paraffin sections were incubated with the primary antibodies against Ki67 (ab15580, 1:100 dilution; Abcam), PCNA, MMP9 (ab76003, 1:200 dilution; Abcam), CDC42 and a biotinylated secondary antibody (ab15580, 1:1,000 dilution; Abcam), followed by incubation with the DAB Detection Kit (Abcam) as per the accompanying protocols.

Statistical analysis

Values were expressed as mean \pm standard deviation

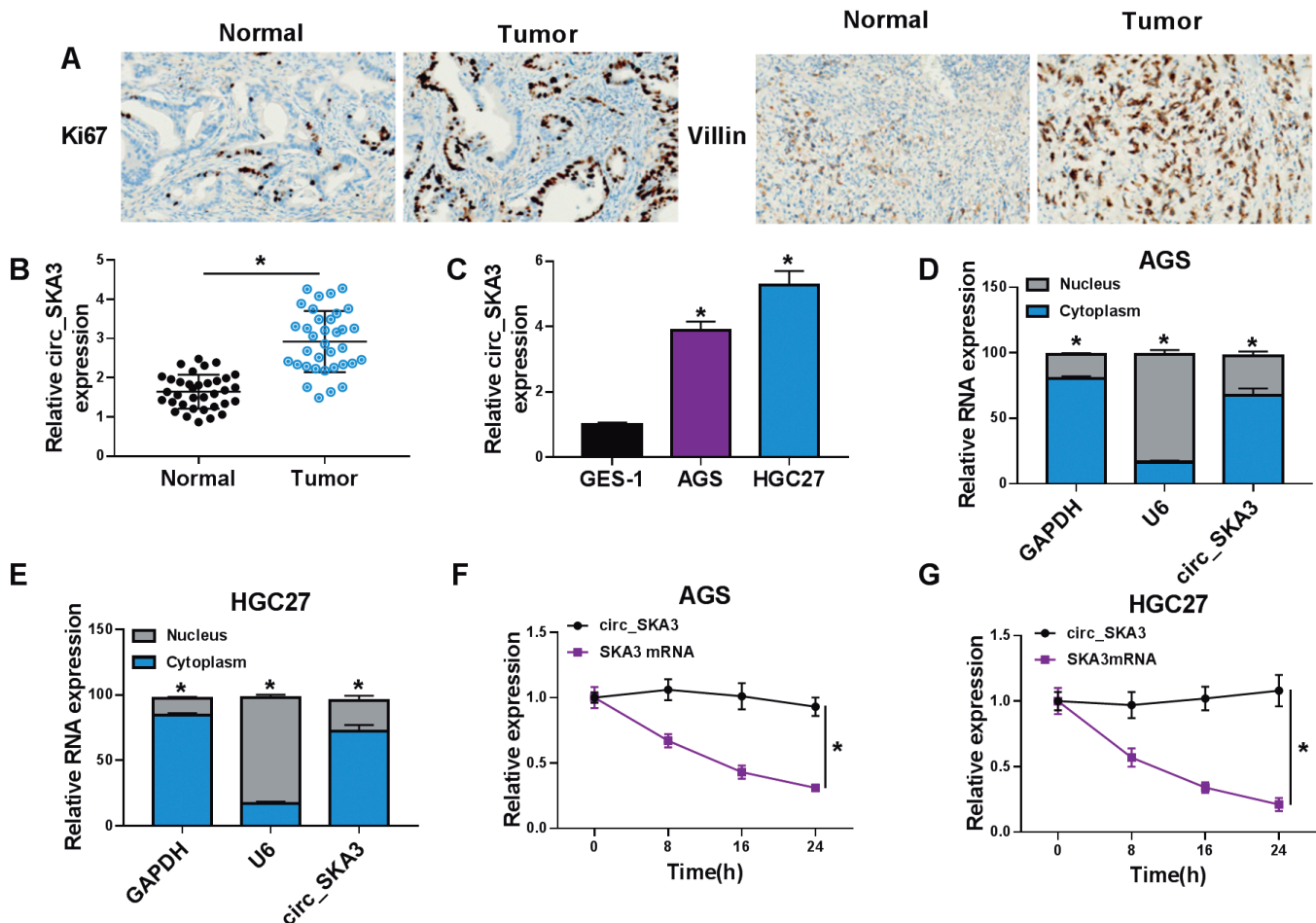


Fig. 1. Overexpression of circ_SKA3 in GC tissues and cells. **A.** Representative immunohistochemical staining of Ki67 and Villin in primary tumor samples and matched normal gastric samples from the same patients. **B.** qRT-PCR for circ_SKA3 expression in a panel of 35 gastric primary tumors and 35 nontumor gastric tissues from the same patients. **C.** Relative circ_SKA3 expression by qRT-PCR in GES-1 gastric epithelial cells, AGS, and HGC27 GC cells. **D, E.** Subcellular localization assays in both AGS and HGC27 cell lines, with GAPDH and U6 as the controls. **F, G.** Actinomycin D assays in both AGS and HGC27 cell lines. * $P < 0.05$.

Effect of circ_SKA3 on GC development

(SD) from 3 independent biological replicates and triplicate experiments. Student's *t*-test was used for the comparison between two groups, and analysis of variance (ANOVA) with Tukey's post hoc test was applied for analysis of three or more groups. The comparative analysis between gastric primary tumors and control tissues was conducted using the Mann-Whitney U test. Pearson's correlation coefficient was used to evaluate the correlations among circ_SKA3, miR-520h, and CDC42 expression in primary gastric tumors. In all these analyses, a $P < 0.05$ was considered significant.

Results

Circ_SKA3 was overexpressed in GC tissues and cell lines

We used qRT-PCR to gauge the expression of

circ_SKA3 in a set of 35 gastric primary tumors paired with nontumor gastric tissues from the same patients. Collected tumor samples had significantly more cells stained for Ki67 and Villin staining than the matched normal controls (Fig. 1A). By contrast, circ_SKA3 was remarkably overexpressed in these tumors (Fig. 1B). In link with the GC tissues, AGS and HGC27 GC cells showed a significant augmentation in circ_SKA3 expression compared with GES-1 gastric epithelial cells (Fig. 1C). To analyze the localization of circ_SKA3 in AGS and HGC27 cells, we adopted a subcellular localization assay. These results showed that circ_SKA3 was mainly present in the cytoplasm of AGS and HGC27 cells (Fig. 1D,E). To determine the stability of circ_SKA3, we carried out the Actinomycin D analysis. Incubation of the cells with Actinomycin D led to a quick reduction in the level of SKA3 linear mRNA, and circ_SKA3 was unusually stable and its level did not reduce in the assayed time frame (Fig. 1F,G).

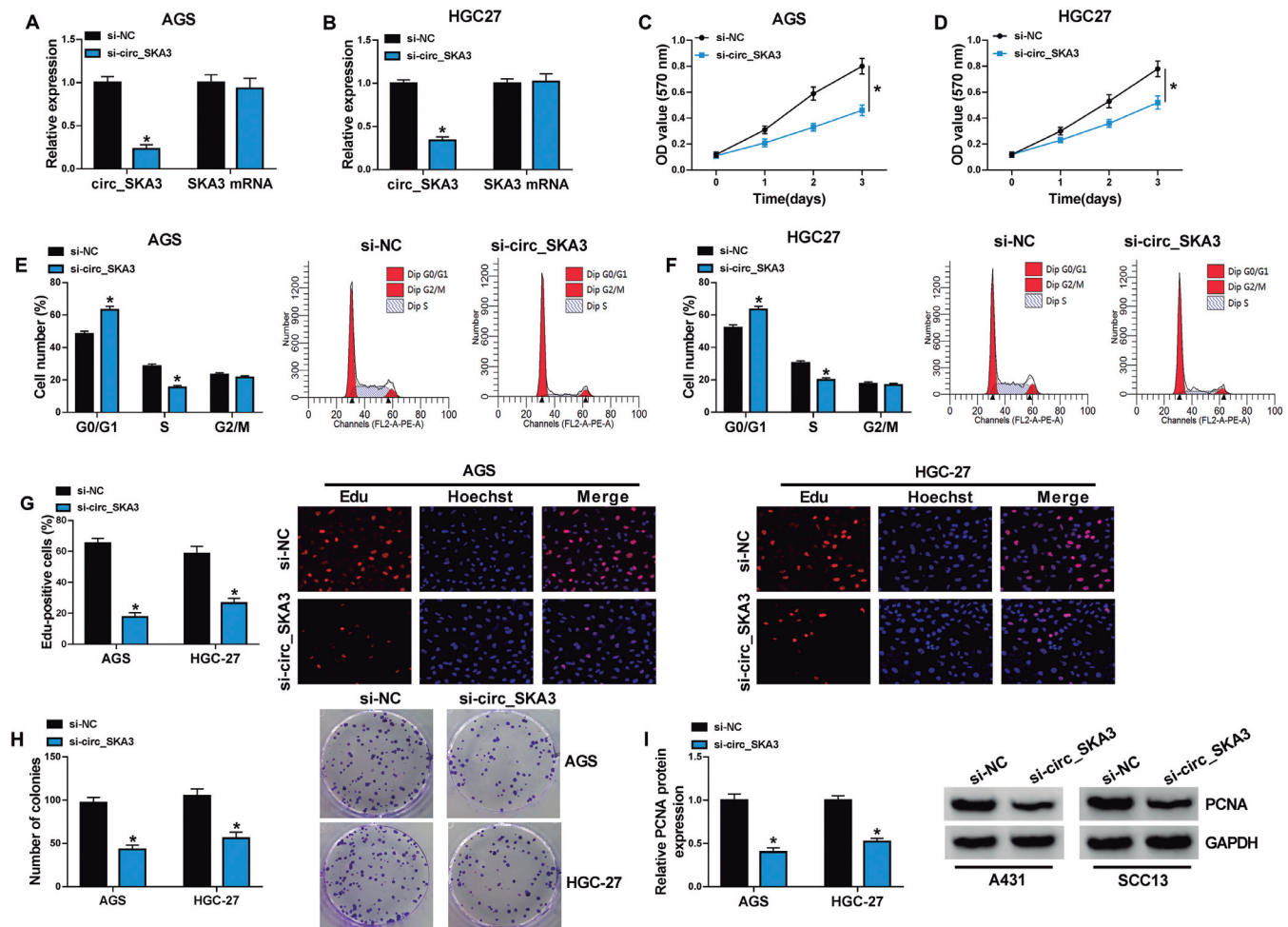


Fig. 2. The down-regulation of circ_SKA3 suppressed cell proliferation, cell cycle progression, and colony formation *in vitro*. AGS and HGC27 cells were transfected with si-circ_SKA3 or si-NC. **A, B.** qRT-PCR for circ_SKA3 and SKA3 linear mRNA levels in transfected cells. **C, D.** Cell proliferation by MTT assay. **E, F.** Representative images depicting a cell cycle distribution assay and cell cycle distribution by flow cytometry. **G.** Representative images depicting a cell proliferation assay and cell proliferation by EdU assay. **H.** Representative images depicting a cell colony formation assay and cell colony formation by colony formation assay. **I.** Representative images depicting a PCNA expression analysis and PCNA expression by western blot. * $P < 0.05$.

Effect of circ_SKA3 on GC development

Silencing of circ_SKA3 suppressed cell proliferation, cell cycle progression, colony formation, migration, invasion, and promoted cell apoptosis *in vitro*

Given the overexpression of circ_SKA3 in GC, we

decided to address its role in controlling the functional behaviors of GC cells *in vitro*. Transfection of siRNA targeting circ_SKA3 (si-circ_SKA3), but not the negative si-NC control, inhibited circ_SKA3 expression by >2 fold in both cell lines (Fig. 2A,B). As expected, si-

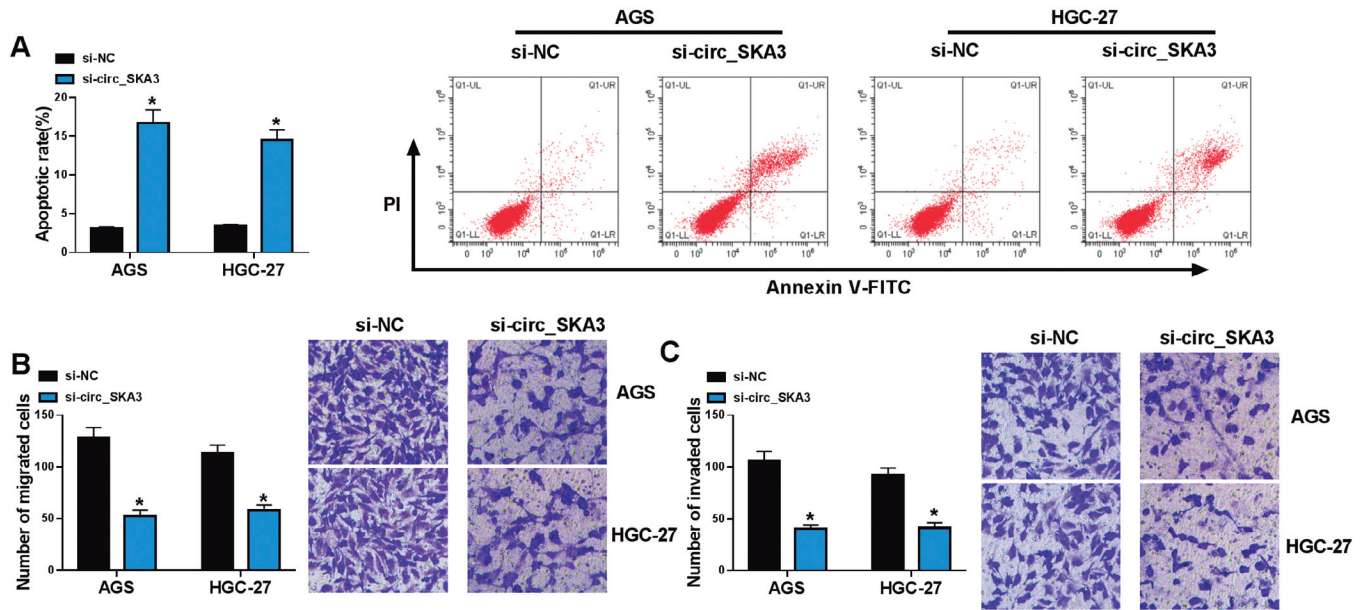


Fig. 3. The down-regulation of circ_SKA3 enhanced cell apoptosis and hindered migration and invasion. AGS and HGC27 cells were transfected with si-circ_SKA3 or si-NC. **A.** Representative images depicting a cell apoptosis assay and cell apoptosis by flow cytometry. **B.** Representative images depicting a cell migration assay and cell migration by transwell assay. **C.** Representative images depicting a cell invasion assay and cell invasion by transwell assay. * $P < 0.05$.

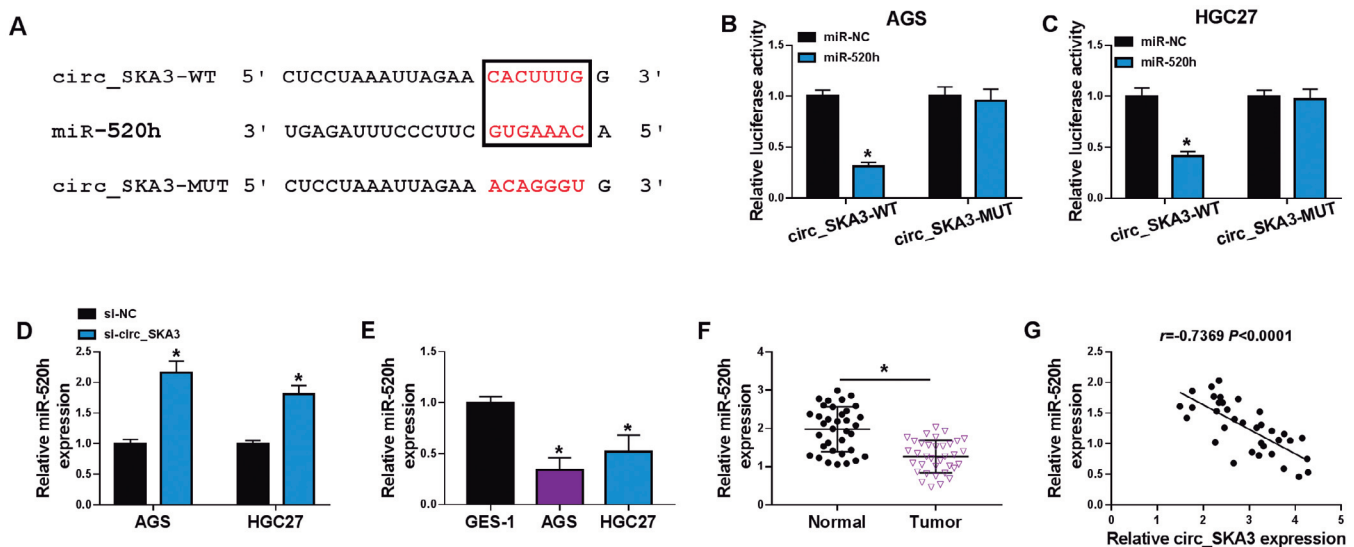


Fig. 4. Circ_SKA3 interacted with miR-520h by directly binding to miR-520h. **A.** Sequence of miR-520h, the putative miR-520h-binding sites within circ_SKA3, and the mutation of the target region. **B.** **C.** Dual-luciferase reporter assays in both AGS and HGC27 cell lines using circ_SKA3 wild-type (circ_SKA3-WT) or mutant (circ_SKA3-MUT) luciferase reporter constructs. **D.** qRT-PCR for miR-520h expression in AGS and HGC27 cells transfected with si-circ_SKA3 or si-NC. **E.** Relative miR-520h level by qRT-PCR in GES-1 gastric epithelial cells, AGS, and HGC27 GC cells. **F.** qRT-PCR for miR-520h expression in a panel of 35 gastric primary tumors and 35 nontumor gastric tissues from the same patients. **G.** Correlation between miR-520h and circ_SKA3 expression in gastric primary tumors. * $P < 0.05$.

Effect of circ_SKA3 on GC development

circ_SKA3 transfection did not cause any significant alteration in the level of the corresponding linear mRNA (Fig. 2A,B). Intriguingly, the down-regulation of circ_SKA3 by si-circ_SKA3 transfection markedly suppressed cell proliferation, cell cycle progression, and cell colony formation (Fig. 2C-H), as well as inhibiting PCNA expression (Fig. 2I) in the two GC cell lines. Conversely, the down-regulation of circ_SKA3 enhanced apoptosis of AGS and HGC27 cells (Fig. 3A). Furthermore, circ_SKA3-silenced cells exhibited suppressed migration (Fig. 3B) and invasion (Fig. 3C) rates compared with the control group.

Circ_SKA3 directly interacted with miR-520h

To elucidate the mechanism of circ_SKA3 function on GC cell behaviors, we interrogated the starBase software to search its targeted miRNAs, and we found a putative complementary sequence for miR-520h within circ_SKA3 (Fig. 4A). To test this possibility, we adopted dual-luciferase reporter assays. Transfection of miR-

520h mimic prominently repressed the luciferase activity of a reporter construct (circ_SKA3-WT) harboring the miR-520h-binding sites, while the mutation of the target region (circ_SKA3-MUT) abolished this effect (Fig. 4B,C), demonstrating the validity of the target sites for interaction. Importantly, circ_SKA3 loss of function clearly increased miR-520h expression in both AGS and HGC27 cell lines (Fig. 4D). Additionally, compared with their counterparts, GC cells and tissues exhibited lower levels of miR-520h (Fig. 4E,F). Interestingly, there existed a strong inverse correlation between miR-520h and circ_SKA3 expression in gastric primary tumors (Fig. 4G).

MiR-520h was a downstream effector of circ_SKA3 function on cell behaviors in vitro

In order to explore whether miR-520h could mediate the function of circ_SKA3 on GC cell behaviors, we specifically silenced miR-520h by miRNA inhibitor (anti-miR-520h) in AGS and HGC27 cells transfected

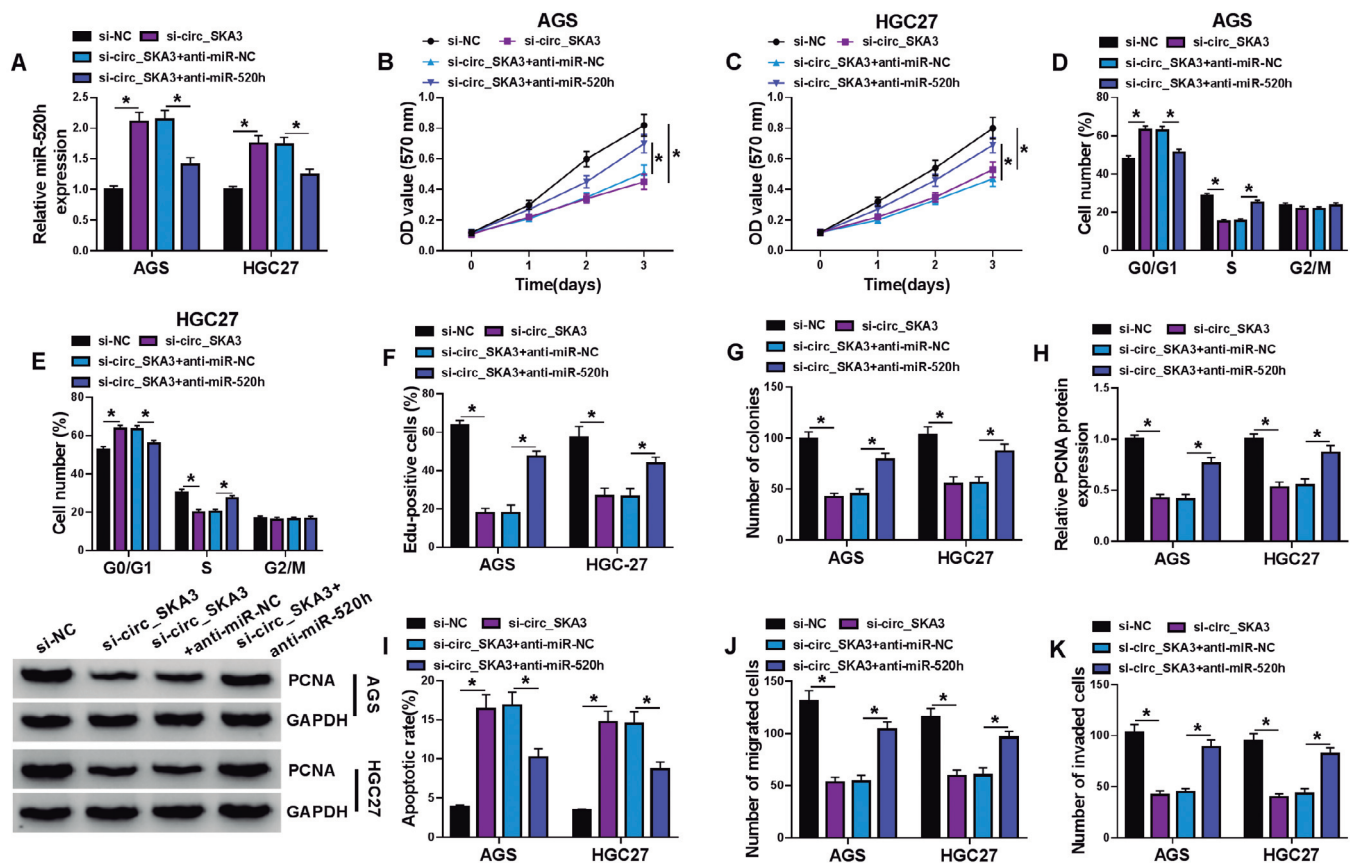


Fig. 5. Circ_SKA3 controlled GC cell behaviors *in vitro* by miR-520h. AGS and HGC27 cells were transfected with si-circ_SKA3, si-NC, si-circ_SKA3+anti-miR-NC or si-circ_SKA3+anti-miR-520h. **A.** Relative miR-520h expression by qRT-PCR in transfected cells. **B, C.** MTT assay for cell proliferation ability. **D, E.** Cell cycle distribution by flow cytometry. **F.** EdU assay for cell proliferation. **G.** Colony formation assay for cell colony formation. **H.** Western blot for PCNA protein level. **I.** Flow cytometry for cell apoptosis. **J.** Cell migration by transwell assay. **K.** Transwell assay for cell invasion. * $P < 0.05$.

Effect of circ_SKA3 on GC development

with si-circ_SKA3 (Fig. 5A). As would be expected, the reduced expression of miR-520h dramatically abrogated the suppression of circ_SKA3 down-regulation on cell

proliferation, cell cycle progression, and colony formation, as well as PCNA protein expression (Fig. 5B-H). Furthermore, the reduced level of miR-520h

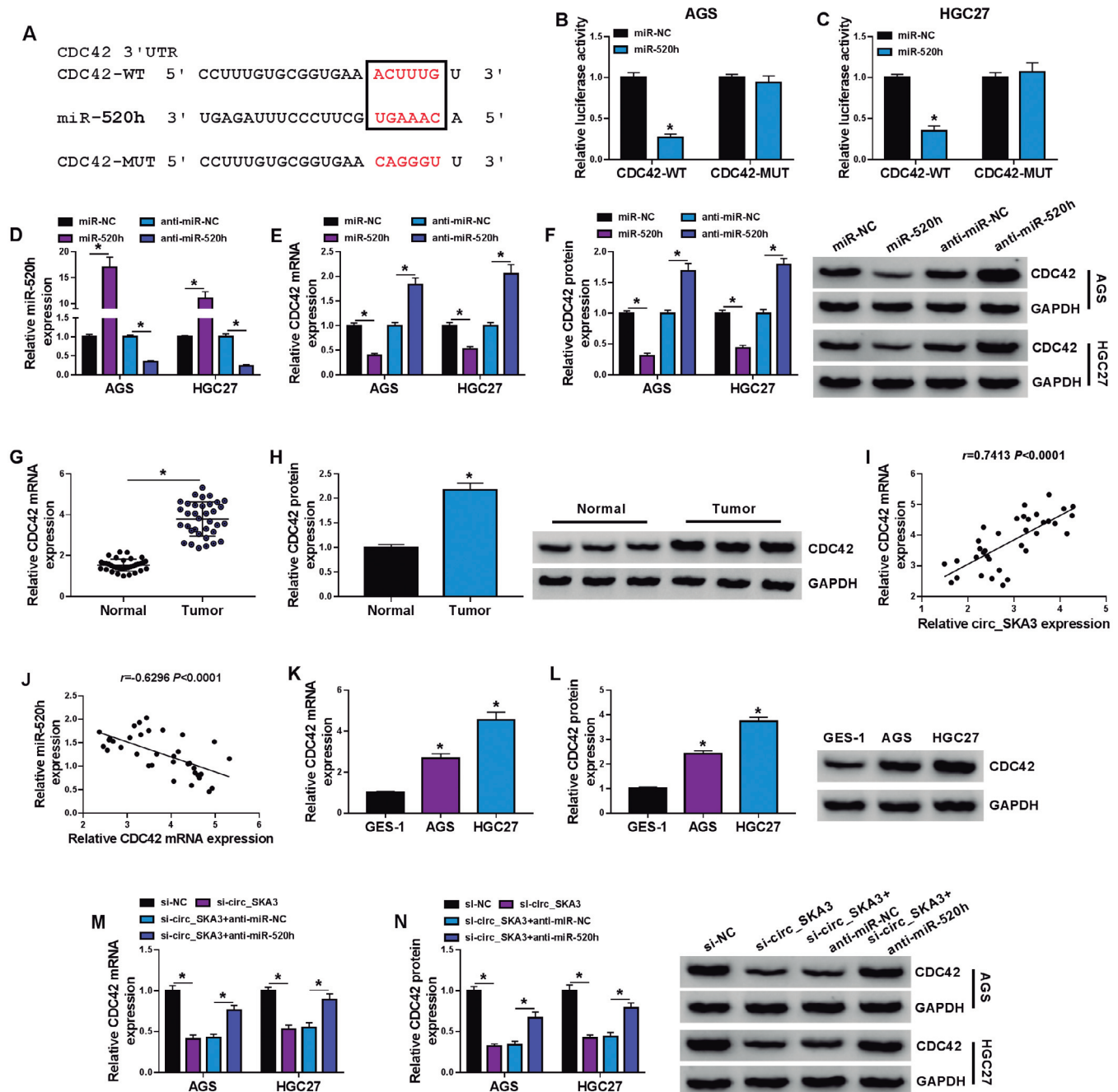


Fig. 6. Circ_SKA3 modulated CDC42 expression by targeting miR-520h. **A**, Sequence of miR-520h, the potential miR-520h-binding sequence with CDC42 3'UTR, and the mutation of the binding sites. **B**, **C**, Dual-luciferase reporter assays in AGS and HGC27 GC cells using the CDC42 3'UTR reporter construct (CDC42-WT) and the mutations in the binding sites (CDC42-MUT). AGS and HGC27 cells were transfected with miR-NC mimic, miR-520h mimic, anti-miR-NC or anti-miR-520h, followed by the assessment of miR-520h expression by qRT-PCR (**D**), CDC42 mRNA level by qRT-PCR (**E**), CDC42 protein level by western blot (**F**). **G**, **H**, CDC42 mRNA and protein levels by qRT-PCR and western blot in a panel of gastric primary tumors and nontumor gastric tissues from the same patients. **I**, **J**, Correlation between CDC42 mRNA level and circ_SKA3 or miR-520h expression in 35 gastric primary tumors. **K**, **L**, qRT-PCR for CDC42 mRNA level and western blot for CDC42 protein level in GES-1 gastric epithelial cells, AGS, and HGC27 GC cells. **M**, **N**, CDC42 mRNA level by qRT-PCR and CDC42 protein level by western blot in cells transfected with si-circ_SKA3, si-NC, si-circ_SKA3+anti-miR-NC or si-circ_SKA3+anti-miR-520h. * $P<0.05$.

Effect of circ_SKA3 on GC development

significantly reversed si-circ_SKA3-mediated proapoptosis (Fig. 5I), anti-migration (Fig. 5J), and anti-invasion (Fig. 5K) effects in both cell lines.

Circ_SKA3 acted as a post-transcriptional regulator of CDC42 through miR-520h

To further understand the role of miR-520h, we searched the starBase database looking for its target mRNAs. Intriguingly, there existed several complementary sites between miR-520h and CDC42 3'UTR (Fig. 6A). To establish the direct relationship between miR-520h and CDC42, we generated CDC42 3'UTR reporter construct (CDC42-WT) and the mutations in the binding sites (CDC42-MUT). Transient transfection of miR-520h mimic induced a >50%

reduction of luciferase activity of CDC42-MUT (Fig. 6B,C). Site-directed mutation (CDC42-MUT) dramatically abrogated the inhibition of miR-520h on reporter gene expression (Fig. 6B,C). To examine whether miR-520h was a post-transcriptional regulator of CDC42, we manipulated miR-520h expression with miR-520h mimic or anti-miR-520h in both AGS and HGC27 cells (Fig. 6D). As expected, the overexpression of miR-520h by miR-520h mimic significantly decreased CDC42 mRNA and protein levels, while the knockdown of miR-520h by anti-miR-520h strongly elevated the levels of CDC42 mRNA and protein in both cell lines (Fig. 6E,F). In addition, compared with the normal controls, GC tissues showed higher levels of CDC42 mRNA and protein (Fig. 6G,H). Importantly, in gastric primary tumors, CDC42 mRNA level positively

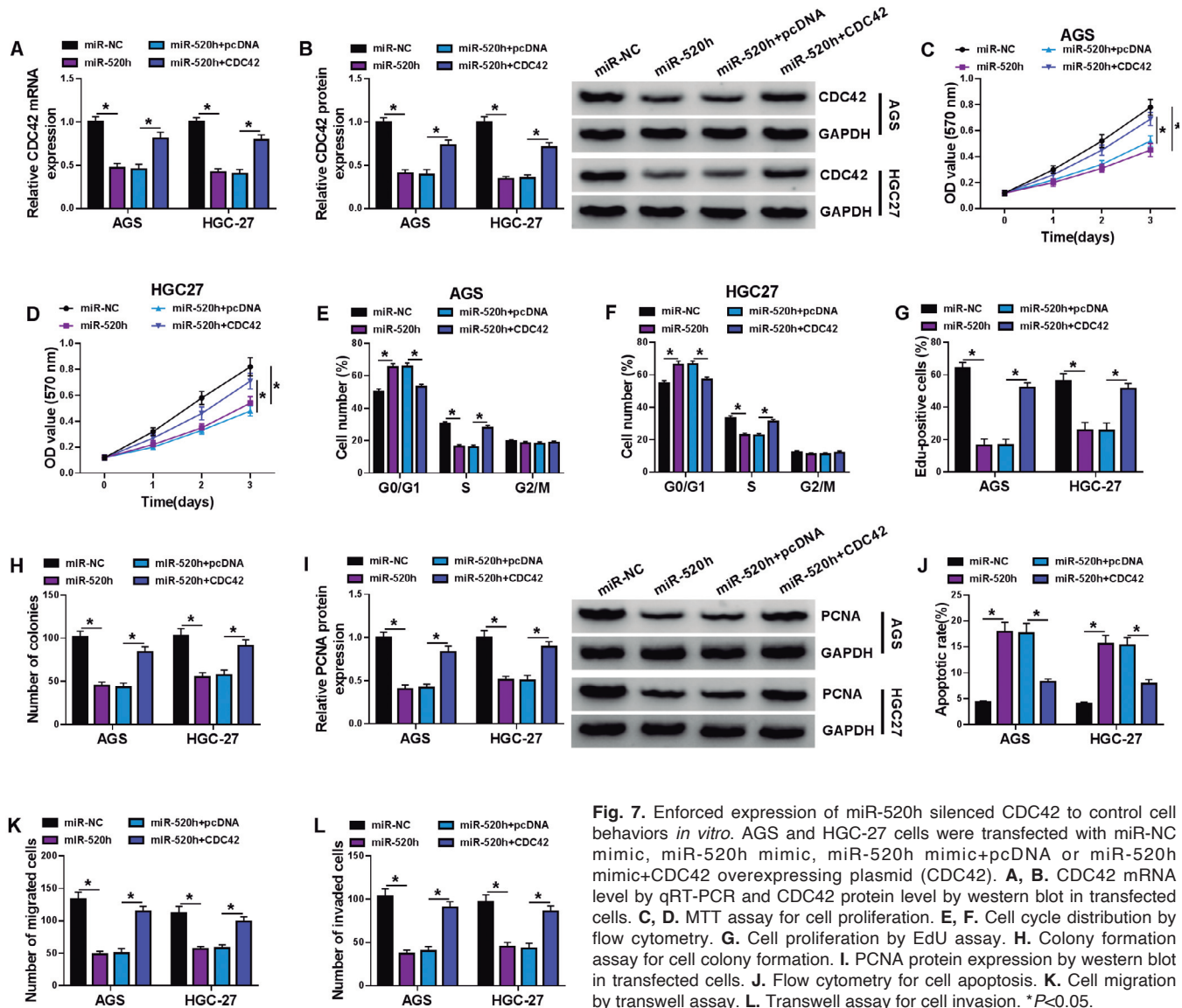


Fig. 7. Enforced expression of miR-520h silenced CDC42 to control cell behaviors *in vitro*. AGS and HGC-27 cells were transfected with miR-NC mimic, miR-520h mimic, miR-520h mimic+pcDNA or miR-520h mimic+CDC42 overexpressing plasmid (CDC42). **A, B.** CDC42 mRNA level by qRT-PCR and CDC42 protein level by western blot in transfected cells. **C, D.** MTT assay for cell proliferation. **E, F.** Cell cycle distribution by flow cytometry. **G.** Cell proliferation by Edu assay. **H.** Colony formation assay for cell colony formation. **I.** PCNA protein expression by western blot in transfected cells. **J.** Flow cytometry for cell apoptosis. **K.** Cell migration by transwell assay. **L.** Transwell assay for cell invasion. * $P < 0.05$.

Effect of circ_SKA3 on GC development

correlated with circ_SKA3 expression and inversely correlated with miR-520h expression (Fig. 6I,J). Consistent with the GC tissues, AGS and HGC27 GC cell lines exhibited higher levels of CDC42 mRNA and protein (Fig. 6K,L). These data together indicated that CDC42 was a direct target of miR-520h.

Then, we wanted to verify whether circ_SKA3 could control the expression of CDC42 in the two GC cell lines. Intriguingly, the silencing of circ_SKA3 by si-circ_SKA3 transfection induced a significant reduction in the levels of CDC42 mRNA and protein (Fig. 6M,N). Furthermore, the suppressive effect was clearly counteracted by anti-miR-520h transfection (Fig. 6M,N), suggesting that circ_SKA3 controlled CDC42 expression through miR-520h.

Enforced expression of miR-520h regulated GC cell behaviors *in vitro* by down-regulating CDC42

Next, we asked how miR-520h modulated GC cell behaviors *in vitro*. Besides the inhibition of CDC42 expression (Fig. 7A,B), the enforced expression of miR-520h by miR-520h mimic transfection remarkably impeded cell proliferation, cell cycle progression, colony formation (Fig. 7C-H), PCNA protein expression (Fig.

7I), and promoted cell apoptosis (Fig. 7J), as well as repressing cell migration (Fig. 7K) and invasion (Fig. 7L) in both AGS and HGC-27 cell lines. In order to establish the importance of CDC42 down-regulation on miR-520h-specific regulation on GC cell behaviors, we performed a rescue experiment by up-regulating CDC42 in miR-520h-overexpressing cells (Fig. 7A,B). Rescue experiments showed that the restored expression of CDC42 significantly abrogated the regulatory impact of miR-520h overexpression on GC cell behaviors (Fig. 7C-L).

Silencing of circ_SKA3 attenuated tumor growth *in vivo*

A pivotal question was whether circ_SKA3 could impact tumor growth *in vivo*. To elucidate this possibility, we injected AGS GC cells stably transduced shRNA-circ_SKA3 (sh-circ_SKA3) or sh-NC control into the nude mice. The sh-circ_SKA3-transduced AGS tumors showed suppressed growth abilities compared with the sh-NC controls (Fig. 8A,B). As expected, the sh-circ_SKA3-transduced xenograft tumors had lower expression of circ_SKA3 compared to the controls (Fig. 8C). Importantly, the down-regulation of circ_SKA3 augmented miR-520h expression and decreased CDC42

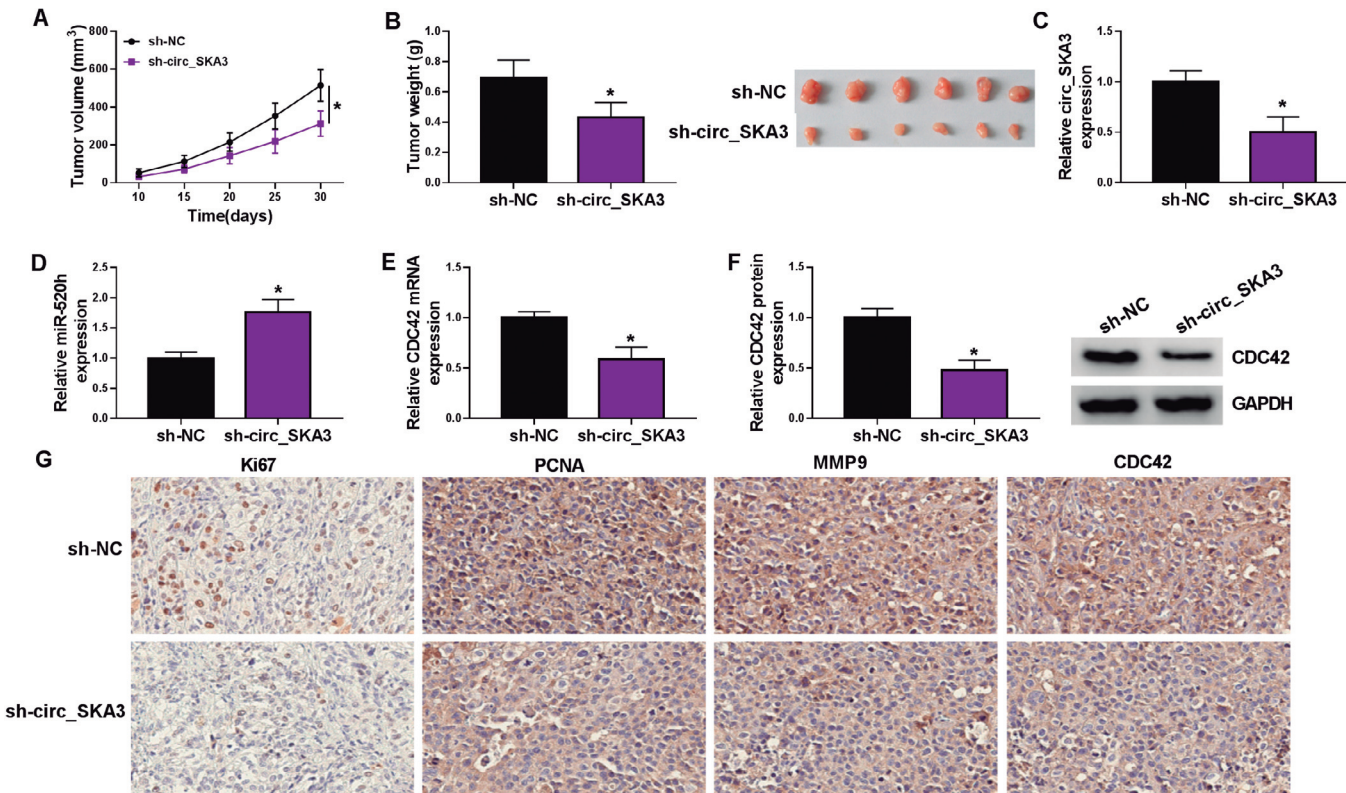


Fig. 8. Circ_SKA3 silencing diminished tumor growth *in vivo*. **A**, Growth curves of the subcutaneous tumors formed by AGS cells transducing with sh-circ_SKA3 or sh-NC. Images and average weight (**B**), circ_SKA3 expression by qRT-PCR (**C**), miR-520h expression by qRT-PCR (**D**), CDC42 mRNA level by qRT-PCR (**E**), CDC42 protein level by western blot (**F**), Ki67, PCNA, MMP9 and CDC42 levels by immunohistochemistry (**G**) of the xenograft tumors at day 30 derived from subcutaneous injections of AGS cells stably transducing with sh-circ_SKA3 or sh-NC. **P*<0.05.

level in the subcutaneous tumors (Fig. 8D-G). Furthermore, immunohistochemistry results showed that the silencing of circ_SKA3 inhibited the protein levels of proliferation marker Ki67, PCNA and motility-related MMP9 in the xenograft tumors (Fig. 8G), demonstrating that the silencing of circ_SKA3 hampered cell growth *in vivo*.

Discussion

Work from the past decade has revealed that dysregulation of circRNAs is involved in gastric tumorigenesis (Fang et al., 2019; Li et al., 2020). Therefore, there is great interest in treatment options to counteract these perturbations of specific circRNAs. Knowing the mechanisms of action of GC-related circRNAs is indispensable for molecularly targeted therapeutics. Considering the promoting effect of circ_SKA3 on GC (Lu et al., 2019; Mo et al., 2020), we wanted to identify its molecular basis, and our results provided a novel regulatory miRNA/mRNA network.

Previous studies uncovered the conflicting actions of miR-520h in human carcinogenesis (Wang et al., 2010; Zhang et al., 2018a; Zhou et al., 2020). These contradictory results might be partially attributed to the different cancer types in these reports, where miR-520h hindered the progression of pancreatic cancer and colorectal cancer (Wang et al., 2010; Zhou et al., 2020) and enhanced epithelial ovarian cancer development (Zhang et al., 2018a). Moreover, miR-520h was able to promote the chemoresistance of breast cancer cells (Su et al., 2017). Conversely, miR-520h was underscored to sensitize cancer cells to doxorubicin in GC and bortezomib in multiple myeloma (Shen et al., 2014; Yuan et al., 2019). Here, we first showed the suppressive effect of miR-520h on GC cell malignant behaviors *in vitro*. More importantly, we first demonstrated that circ_SKA3 directly bound to miR-520h, and miR-520h was a downstream effector of circ_SKA3 function in GC.

CDC42, a member of the Rho GTPase family, has been recognized as a potent oncogene in every major cancer type by controlling important cellular processes (Maldonado and Dharmawardhane, 2018; Xiao et al., 2018). Inhibition of CDC42 is widely proposed as a potential point for the development of novel anti-tumor agents. Moreover, CDC42 has been established as a potent driver in gastric tumorigenesis (Du et al., 2016; Zhu et al., 2019). Enhanced CDC42 activity was reported to be associated with poor prognosis of patients with advanced GC. Here, we first validated that CDC42 was a functional target of miR-520h in regulating GC cell behaviors. Similarly, several other miRNAs, such as miR-148-3p and miR-137, functioned as promising suppressors in GC by silencing CDC42. More importantly, we first highlighted the role of circ_SKA3 as a post-transcriptional regulator of CDC42 through miR-520h. A recent study showed that circ_SKA3 contributed to GC development by targeting miR-326-3p

(Mo et al., 2020). With these findings, we inferred that miR-520h and miR-326-3p were two parallel mediators of circ_SKA3 function in gastric tumorigenesis. There may be other molecular mechanisms that remain to be identified in the oncogenic role of circ_SKA3 in GC development. Additionally, the direct evidence between the miR-520h/CDC42 axis and circ_SKA3-mediated GC development *in vivo* is lacking at present, which will be investigated in further work.

In summary, the findings in this study provided a strong molecular determinant, the miR-520h/CDC42 axis, for the oncogenic role of circ_SKA3 in GC. Our findings established a notion that targeting circ_SKA3 might be a new anti-cancer strategy for GC.

Acknowledgements. Not applicable.

Ethics approval and consent to participate. The present study was approved by the ethical review committee of Suizhou central hospital. Written informed consent was obtained from all enrolled patients.

Consent for publication. Patients agree to participate in this work.

Availability of data and materials. The analyzed data sets generated during the present study are available from the corresponding author on reasonable request.

Competing interests. The authors declare that they have no competing interests.

Funding. No funding was received.

Authors' contribution. All authors made substantial contributions to conception and design, acquisition of the data, or analysis and interpretation of the data; took part in drafting the article or revising it critically for important intellectual content; gave final approval of the revision to be published; and agree to be accountable for all aspect of the work.

References

- Alessandrini L., Manchi M., De Re V., Dolcetti R. and Canzonieri V. (2018). Proposed molecular and miRNA classification of gastric cancer. *Int. J. Mol. Sci.* 19, 1683.
- Bray F., Ferlay J., Soerjomataram I., Siegel R.L., Torre L.A. and Jemal A. (2018). Global cancer statistics 2018: GLOBOCAN estimates of incidence and mortality worldwide for 36 cancers in 185 countries. *CA Cancer J. Clin.* 68, 394-424.
- Chen H., Liang C., Wang X., Liu Y., Yang Z., Shen M., Han C. and Ren C. (2020). The prognostic value of circRNAs for gastric cancer: A systematic review and meta-analysis. *Cancer Med.* 9, 9096-9106.
- da Silva Oliveira K.C., Thomaz Araújo T.M., Albuquerque C.I., Barata G.A., Gigek C.O., Leal M.F., Wisniewski F., Rodrigues Mello Junior F.A., Khayat A.S., de Assumpção P.P., Rodriguez Burbano R.M., Cardoso Smith M. and Queiroz Calcagno D. (2016). Role of miRNAs and their potential to be useful as diagnostic and prognostic biomarkers in gastric cancer. *World J. Gastroenterol.* 22, 7951-7962.
- Dori M. and Bicciato S. (2019). Integration of bioinformatic predictions and experimental data to identify circRNA-miRNA associations. *Genes (Basel)* 10, 642.
- Du D.S., Yang X.Z., Wang Q., Dai W.J., Kuai W.X., Liu Y.L., Chu D. and Tang X.J. (2016). Effects of CDC42 on the proliferation and invasion of gastric cancer cells. *Mol. Med. Rep.* 13, 550-554.
- Fang X., Wen J., Sun M., Yuan Y. and Xu Q. (2019). CircRNAs and its

- relationship with gastric cancer. *J. Cancer* 10, 6105-6113.
- Jaca A., Govender P., Lockett M. and Naidoo R. (2017). The role of miRNA-21 and epithelial mesenchymal transition (EMT) process in colorectal cancer. *J. Clin. Pathol.* 70, 331-356.
- Korpál M., Ell B.J., Buffa F.M., Ibrahim T., Blanco M.A., Celià-Terrassa T., Mercatali L., Khan Z., Goodarzi H., Hua Y., Wei Y., Hu G., Garcia B.A., Ragoussis J., Amadori D., Harris A.L. and Kang Y. (2011). Direct targeting of Sec23a by miR-200s influences cancer cell secretome and promotes metastatic colonization. *Nat. Med.* 17, 1101-1108.
- Kristensen L.S., Andersen M.S., Stagsted L.V.W., Ebbesen K.K., Hansen T.B. and Kjems J. (2019). The biogenesis, biology and characterization of circular RNAs. *Nat. Rev. Genet.* 20, 675-691.
- Li R., Jiang J., Shi H., Qian H., Zhang X. and Xu W. (2020). CircRNA: a rising star in gastric cancer. *Cell. Mol. Life Sci.* 77, 1661-1680.
- Lu J., Zhang P.Y., Xie J.W., Wang J.B., Lin J.X., Chen Q.Y., Cao L.L., Huang C.M., Li P. and Zheng C.H. (2019). Hsa_circ_0000467 promotes cancer progression and serves as a diagnostic and prognostic biomarker for gastric cancer. *J. Clin. Lab. Anal.* 33, e22726.
- Maldonado M.D.M. and Dharmawardhane S. (2018). Targeting Rac and Cdc42 GTPases in cancer. *Cancer Res.* 78, 3101-3111.
- Mo W.L., Jiang J.T., Zhang L., Lu Q.C., Li J., Gu W.D., Cheng Y. and Wang H.T. (2020). Circular RNA hsa_circ_0000467 promotes the development of gastric cancer by competitively binding to microRNA miR-326-3p. *Biomed. Res. Int.* 2020, 4030826.
- Qi R., Wang D.T., Xing L.F. and Wu Z.J. (2018). miRNA-21 promotes gastric cancer growth by adjusting prostaglandin E2. *Eur. Rev. Med. Pharmacol. Sci.* 22, 1929-1936.
- Shen Q., Yao Q., Sun J., Feng L., Lu H., Ma Y., Liu L., Wang F., Li J., Yue Y., Jin H. and Wang X. (2014). Downregulation of histone deacetylase 1 by microRNA-520h contributes to the chemotherapeutic effect of doxorubicin. *FEBS Lett.* 588, 184-191.
- Smid D., Kulda V., Srbecka K., Kubackova D., Dolezal J., Daum O., Kucera R., Topolcan O., Treska V., Skalicky T. and Pesta M. (2016). Tissue microRNAs as predictive markers for gastric cancer patients undergoing palliative chemotherapy. *Int. J. Oncol.* 48, 2693-2703.
- Smyth E.C., Nilsson M., Grabsch H.I., van Grieken N.C. and Lordick F. (2020). Gastric cancer. *Lancet* 396, 635-648.
- Su C.M., Wang M.Y., Hong C.C., Chen H.A., Su Y.H., Wu C.H., Huang M.T., Chang Y.W., Jiang S.S., Sung S.Y., Chang J.-Y., Chen L.-T., Chen P.-S. and Su J.-L. (2017). miR-520h is crucial for DAPK2 regulation and breast cancer progression. *Oncogene* 36, 5770.
- Tian S. and Yu H. (2017). Atractylenolide II inhibits proliferation, motility and induces apoptosis in human gastric carcinoma cell lines HGC-27 and AGS. *Molecules* 22, 1886.
- Wang F., Xue X., Wei J., An Y., Yao J., Cai H., Wu J., Dai C., Qian Z., Xu Z. and Miao Y. (2010). hsa-miR-520h downregulates ABCG2 in pancreatic cancer cells to inhibit migration, invasion, and side populations. *Br J. Cancer* 103, 567-574.
- Wang F., Qu N., Peng J., Yue C., Yuan L. and Yuan Y. (2017). CagA promotes proliferation and inhibits apoptosis of GES-1 cells by upregulating TRAF1/4-1BB. *Mol. Med. Rep.* 16, 1262-1268.
- Wang S., Zhang X., Li Z., Wang W., Li B., Huang X., Sun G., Xu J., Li Q., Xu Z., Xia Y., Wang L., Zhang Q., Li Q., Zhang L., Chen J., Wu Y., Cao J., Xu P., Zhang D., Xu H. and Xu Z. (2019). Circular RNA profile identifies circOSBPL10 as an oncogenic factor and prognostic marker in gastric cancer. *Oncogene* 38, 6985-7001.
- Xiao X.H., Lv L.C., Duan J., Wu Y.M., He S.J., Hu Z.Z. and Xiong L.X. (2018). Regulating Cdc42 and its signaling pathways in cancer: Small molecules and MicroRNA as new treatment candidates. *Molecules* 23, 787.
- Yuan X., Ma R., Yang S., Jiang L., Wang Z., Zhu Z. and Li H. (2019). miR-520g and miR-520h overcome bortezomib resistance in multiple myeloma via suppressing APE1. *Cell Cycle* 18, 1660-1669.
- Zhang J., Liu W., Shen F., Ma X., Liu X., Tian F., Zeng W., Xi X. and Lin Y. (2018a). The activation of microRNA-520h-associated TGF- β 1/c-Myb/Smad7 axis promotes epithelial ovarian cancer progression. *Cell Death Dis.* 9, 884.
- Zhang X., Li Z., Xuan Z., Xu P., Wang W., Chen Z., Wang S., Sun G., Xu J. and Xu Z. (2018b). Novel role of miR-133a-3p in repressing gastric cancer growth and metastasis via blocking autophagy-mediated glutaminolysis. *J. Exp. Clin. Cancer Res.* 37, 320.
- Zhang L., Song X., Chen X., Wang Q., Zheng X., Wu C. and Jiang J. (2019). Circular RNA CircCACTIN promotes gastric cancer progression by sponging MiR-331-3p and regulating TGFBR1 expression. *Int. J. Biol. Sci.* 15, 1091-1103.
- Zhong S., Wang J., Hou J., Zhang Q., Xu H., Hu J., Zhao J. and Feng J. (2018). Circular RNA hsa_circ_0000993 inhibits metastasis of gastric cancer cells. *Epigenomics* 10, 1301-1313.
- Zhou T., Wu L., Ma N., Tang F., Zong Z. and Chen S. (2020). LncRNA PART1 regulates colorectal cancer via targeting miR-150-5p/miR-520h/CTNNB1 and activating Wnt/ β -catenin pathway. *Int. J. Biochem. Cell Biol.* 118, 105637.
- Zhu Z., Yu Z., Rong Z., Luo Z., Zhang J., Qiu Z. and Huang C. (2019). The novel GINS4 axis promotes gastric cancer growth and progression by activating Rac1 and CDC42. *Theranostics* 9, 8294-8311.